Thermal and luminous investigations of a pcLED based refrigerating liquid prototype

Luigi Colombo [a], Alberto Dolara [a], Stefania Guzzetti [a], George Cristian Lazaroiu [b,*], Sonia Leva [a], Andrea Lucchini [a]

[a] Department of Energy, Politecnico di Milano, Via Lambruschini 4, 20156 Milan, Italy
[b] Department of Power Systems, University Politehnica of Bucharest, Splaiul Independentei 313, 060042 Bucharest, Romania

Received 23 December 2013
Accepted 6 June 2014
Available online 14 June 2014

1. Introduction

Over the last few years, the light-emitting diodes (LEDs) are attracting the attention of lighting applications industry, like LCD displays, visual indicators in instruments and computers, interior and exterior automotive lighting including headlights, displays, signals and luminaries, due to their lower power consumption and long lifetime [1,2]. In fact, due to rapid technological development, the luminous efficiency of LED has grown beyond 120 lm/W in commercial products. The LEDs guarantee important energy savings with respect to the most common light sources, like incandescent and halogen lamps [3]. In addition, they are also considered one of the most valuable light sources in 21st century [4,5] due to their longer lifespan, lower power consumption and smaller size with respect to traditional lighting.

Still, their use presents a thermal issue, since about 70% of their total energy consumption is wasted as heat [6]. The heat management is an important challenge as the junction temperature increase determines the decrease of LEDs' lifetime, the failure of the

* Corresponding author. Tel.: +40 724528546.
E-mail addresses: luigi.colombo@polimi.it (L. Colombo), alberto.dolara@mail.polimi.it (A. Dolara), stefania.guzzetti@polimi.it (S. Guzzetti), clazaroiu@yahoo.com (G.C. Lazaroiu), sonia.leva@polimi.it (S. Leva), andrea.lucchini@polimi.it (A. Lucchini).

devices, the shift of color spectrum, and lower operational efficiency. Without appropriate thermal management, the efficiency of LEDs can be reduced from a theoretical 90% to values as low as 20% [7]. Thus, the efficient thermal design is essential for improving the LED's performances.

The thermal management and optical performance of an array package assembly in air, with high-power white LEDs, in various placement algorithms, is investigated in Ref. [8]. The analysis of thermal interaction between LED array and placement design was conducted. The thermal performance and design of LED lighting source (with 18 red LED packages) and their impact on optimal performances of LED module is investigated in Ref. [9]. Two thermal schemes, application of thermal grease and of aluminum case with a surface in heat sink type, are analyzed. The obtained results revealed that improvements of light output power and radiant intensity can be achieved.

The thermal study of a 3 W blue LED, with thermal paste and mylar tape as interface materials, by utilizing the dual interface method is conducted in Ref. [9]. The thermal analysis of blue LED in air and with water flow as cooling system was carried out. The variation of optical power with junction temperature and with applied forward current, for the still air environment, was investigated. Ching and Devarajan applied the dual interface method for determining the junction-to-board thermal resistance for high power infrared LEDs, performing thermal measurements and optical test in case of thermal paste and thermal tape as interface materials [10].

The blue LED covered with a phosphor layer (realizing a phosphor converted LED – pcLED), transforms the blue light into white light [11]. The phenomenon of phosphor self-heating was investigated regarding the effect of phosphor layer relative position in LED packaging [12], the thermal and optical interaction of phosphor-based white LEDs [13], the hot-spot location in high power phosphor converted white LEDs [14]. Luo et al. [15] investigated the phosphor self-heating in the multiple high power LEDs modules. The phosphor mixture layer was coated on LED chips mounted on a heat sink cooled by a fan. Huang et al. [16] developed an electric-heat-optical system dynamics model of a white LED lamp. The influence of driving current and variation of ambient temperature on junction temperature, for a lighting module connected to a heat sink in air, is investigated. Li et al. [17] proposed a thermal resistance analog model for an integrated chip-on-board LED chip with a loop heat pipe heat sink with parallel condensers for LED cooling. A thermal resistance network model for high-power LED arrays fabricated on InGaN/sapphire chips, with 2 active cooling solutions using water as refrigerant, was proposed in Ref. [18]. The junction temperature calculations for different inlet flow rates in the cold plates were carried on.

A new heat management application of a refrigerating liquid integrated within a fabricated prototype is proposed and investigated in Refs. [19], where an aluminum case with white LEDs placed on its bottom was gradually filled with a silicon oil. The conducted experiments revealed that the best thermal performances of the prototype were achieved by totally submersing the white LEDs into the dielectric refrigerant. However, the configuration was reducing the light characteristics, as the wavelengths in the range 530–630 nm were cut when the luminous radiation passed through the liquid.

In this paper, the thermal and optical performances of a new LEDs prototype are investigated. The fabricated prototype consists of blue LEDs and uses as refrigerating liquid the silicon oil. The luminous characteristics and thermal performances of the new configuration are experimentally investigated. The obtained results are used for developing a thermal model of the proposed LED heat management solution.

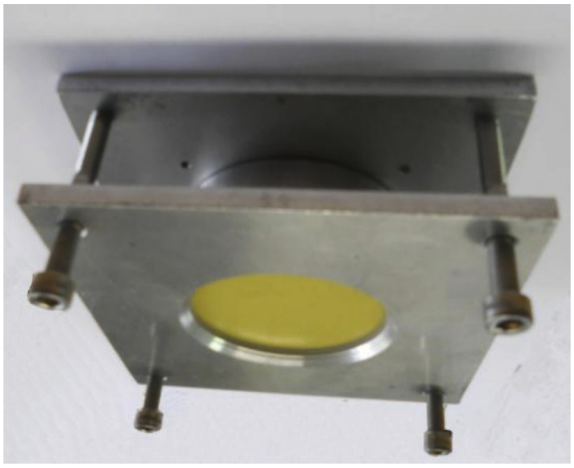

Fig. 1. Fabricated prototype.

2. Fabrication of blue LEDs prototype

The silicon fluid, used as refrigerating agent in Refs. [19], improves the thermal conditions of the LEDs system (the junction temperature decreases as the level of refrigerating liquid increases). Still, important variations of the luminous radiation are occurring. To overcome this bottleneck, the aforementioned configuration can be modified by changing the dielectric fluid filling the case, or by modifying the system's structure. In this paper, the second approach is addressed.

The new proposed prototype of the LED lamp is illustrated in Fig. 1. The 3D model exploded of the fabricated prototype is shown in Fig. 2. The components, from top to the bottom, are: 1-the removable heat sink, 2-the PCB (printed circuit board) LED (6 high power LUXEON Rebel ES Royal blue LEDs, 700 mA, 12.7 W, by General Luminare), 3-the upper closing plate, 4-the silicone gasket, 5-the lateral surface of the fluid enclosure, 6-the glass with

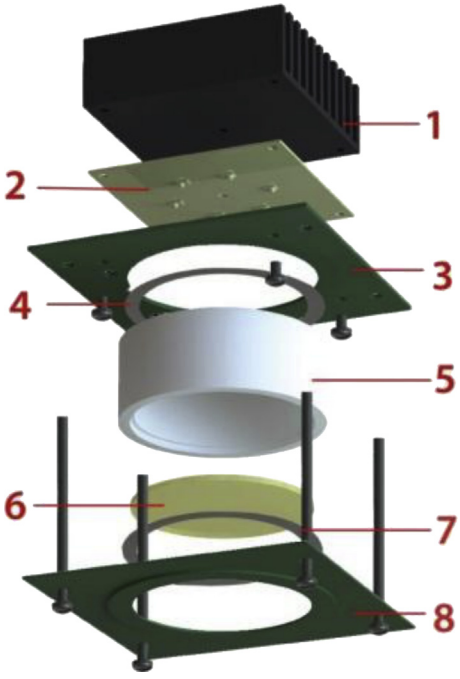

Fig. 2. 3D model exploded of the prototype.

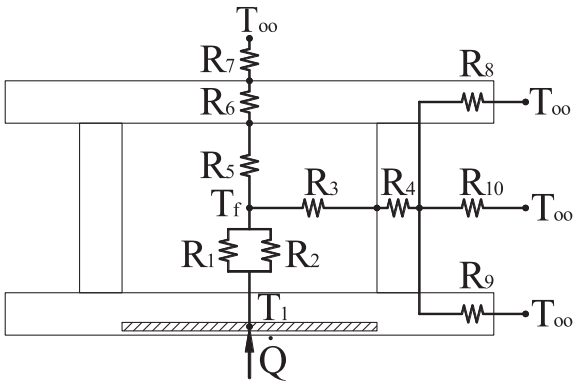

Fig. 3. Thermal network model of the new LED prototype.

phosphor cover (Round ChromaLit™ Phosphor Element 3000 K, 80 CRI, by Intematix), 7-the silicone gasket, 8-the lower closing plate.

The most important elements of the prototype, that characterize the studied LED system, are:

- the polydimethyl silicon fluid (DOW corning 561 Silicon fluid [20]) that acts as refrigerant system;
- the glass with phosphor cover to convert the blue light into white light;
- the blue LEDs designed specifically for use in remote phosphor white light applications; dominant wavelength $\lambda_D = 440–460$ nm.

The use of blue LEDs, whose luminous radiation is not influenced by liquid, allows to overcome the drawback of white LEDs immersed in the refrigerating liquid due to the cutting of luminous radiation wavelengths in the range 530–630 nm. The white light is obtained deposing a phosphor layer with suitable spectral characteristics directly on the inner surface of the glass cover. The other components are required to realize the cylinder that can be filled with liquid or air.

The new proposed configuration is investigated by setting up a thermal model, and through performed experimental tests.

3. Thermal modeling and results

A steady state model based on thermal resistance network allows us to estimate the LED prototype operating temperature and to assess the influence of various geometrical/physical parameters. Assuming axial symmetry, a simplified representation of the main heat flow paths is shown in Fig. 3, where all the thermal resistances are displayed. In Fig. 3, T_1 is the junction temperature, T_f is the silicon fluid temperature, and T_∞ is the ambient air temperature. The thermal resistances R_1 and R_2 account for the convective heat transfer from the LEDs to both the ambient air and to the fluid, within the enclosure, through the PCB. The PCB can be separated in Ring 1 and Ring 2 by the circle ideally connecting the electronic devices, as shown in Fig. 4. Under the assumption of axial symmetry, each ring behaves as a circular fin with the root at the LED temperature. Hence, the associated thermal resistance is given by Ref. [21]:

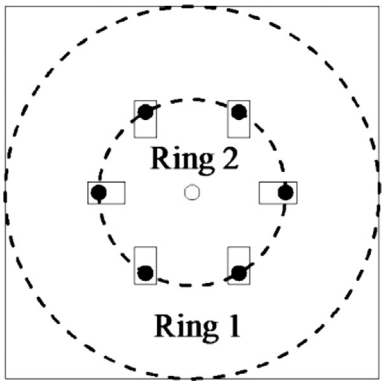

Fig. 4. Schematic of the PCB.

$$R_n = \frac{1}{\eta_f \cdot h_{tot} \cdot A_n}, \quad n = 1,2 \tag{1}$$

where A is the heat transfer area, and η_f is the fin efficiency defined as:

$$\eta_f = \frac{2 \cdot r_i}{m \cdot \left(r_e^2 - r_i^2\right)} \cdot \frac{K_1(mr_i) \cdot I_1(mr_e) - I_1(mr_i) \cdot K_1(mr_e)}{K_0(mr_i) \cdot I_1(mr_e) - I_0(mr_i) \cdot K_1(mr_e)} \tag{2}$$

where I_0 and K_0 are the 0th order Bessel modified functions of the first and second kind, respectively; I_1 and K_1 are the 1st order Bessel modified functions of the first and second kind, respectively; r_i and r_e are inner and outer radiuses; m is the fin parameter expressed as:

$$m = \sqrt{\frac{2 \cdot h_{tot}}{k_{FR-4} \cdot t}} \tag{3}$$

where t is the PCB thickness, $k_{FR\text{-}4}$ is the thermal conductivity of the PCB material (mainly FR-4), and h_{tot} is the total heat transfer coefficient as the sum of average convection heat transfer coefficients on both sides of the PCB. These convective heat transfer coefficients are calculated from suitable correlations.

The resistances R_3 and R_5 account for the convective radial and axial heat transfer from fluid in the case to the internal side of the enclosure, respectively. Their general definition is [21]:

$$R_{conv} = \frac{1}{h \cdot A} \tag{4}$$

where h is the heat transfer coefficient calculated from suitable correlations according to the particular geometry and the cooling fluid. The resistances R_4 accounts for conduction heat transfer of the aluminum case, and R_6 accounts for conduction of the phosphor glass:

$$R_4 = \frac{1}{2 \cdot \pi \cdot k_{Al} \cdot H} \cdot \ln \frac{r_e}{r_i} \tag{5}$$

$$R_6 = \frac{L}{k_p \cdot A} \tag{6}$$

where H is the wall height, and L is the thickness of the plastic layer.

The resistances R_7 and R_{10} account for heat transfer from the external side phosphor glass and the external wall of aluminum case, respectively, and the ambient. The resistances are generally defined by Eq. (4), but the heat transfer coefficient is, in this case, the sum of the convective heat transfer coefficient, taken from suitable correlations, and the radiant heat transfer coefficient expressed by linearization as:

$$h_{rad} = 4 \cdot \varepsilon \cdot \sigma \cdot T_w^3 \tag{7}$$

where ε is the surface emissivity, σ is the Stefan–Boltzmann constant, and T_w is the wall absolute temperature.

Table 1
Thermal properties of the polydimethyl silicon fluid and geometric sizes of the prototype.

Quantity	Unit	Value
FR-4 thermal conductivity	$W\ m^{-1}\ K^{-1}$	1
Aluminum thermal conductivity	$W\ m^{-1}\ K^{-1}$	170
Dow Corning 561 thermal conductivity	$W\ m^{-1}\ K^{-1}$	0.15
Dow Corning 561 isobaric expansion coefficient	K^{-1}	$1.04 \cdot 10^{-3}$
Dow Corning 561 kinematic viscosity	$m^2\ s^{-1}$	$2 \cdot 10^{-5}$
Dow Corning 561 Prandtl number	–	182
Surface emissivity	–	0.9
Board thickness	m	$1.0 \cdot 10^{-3}$
Inner radius for R_1	m	$1.0 \cdot 10^{-3}$
Outer radius for R_1	m	$1.5 \cdot 10^{-2}$
Inner radius for R_2	m	$1.5 \cdot 10^{-2}$
Outer radius for R_2	m	$2.5 \cdot 10^{-2}$
Wall height for R_4	m	$5.0 \cdot 10^{-2}$
Inner radius for R_4	m	$2.5 \cdot 10^{-2}$
Outer radius for R_4	m	$3.0 \cdot 10^{-2}$
Thickness of the plastic window for R_6	m	$3.0 \cdot 10^{-3}$
Inner radius for R_8 and R_9	m	$2.5 \cdot 10^{-2}$
Outer radius for R_8 and R_9	m	$6.0 \cdot 10^{-2}$

Table 2
Thermal resistances.

		Manufacturer data	DC-561	Relative difference (DC-561 to manufacturer)
R_{PCB}	[K/W]	21	14.1	−32.9%
R_{axial}	[K/W]	–	65.1	–
R_{radial}	[K/W]	–	3.0	–
R_{tot}	[K/W]	≥21	16.9	−19.5% minimum

The resistances R_8 and R_9 account for the heat transfer through the aluminum mounting flanges. In the assumed hypothesis of axial symmetry, these resistances can be considered as circular fins and modeled as described by Eq. (1). The four screws, connecting the two flanges for sealing the case, act as thermal bridges. Within the present analysis, the screws are neglected as preliminary thermographic measurements revealed that these are practically at ambient temperature.

The thermal resistances expressed above involve a convective heat transfer coefficient. As free convection occurs in usual operating conditions, the convective heat transfer coefficient can be calculated from correlations of general form [21]:

$$Nu = C \cdot Ra^n \tag{8}$$

where Nu is the Nusselt number referred to a characteristic length L_c, expressed as:

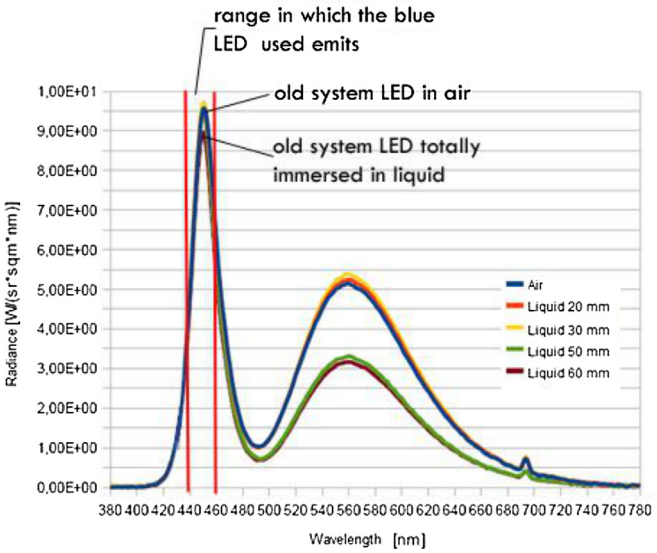

Fig. 6. Variation of radiance, for white LEDs with different refrigerating liquid level heights and for the blue LEDs of the new fabricated prototype.

$$Nu = \frac{h \cdot L_c}{k} \tag{9}$$

C and n are constants depending on the flow regime as well as wall geometry; Ra is the Rayleigh number referred to the same characteristic length and given by:

$$Ra = \frac{g \cdot \beta \cdot \Delta T_c \cdot L_c^3}{\nu \cdot \alpha} \tag{10}$$

where g is the gravitational acceleration, β is the isobaric expansion coefficient, ΔT_c is the wall-fluid temperature difference, ν is the kinematic viscosity, and α is the thermal diffusivity.

The thermal properties of the polydimethyl silicon fluid [20] and geometric sizes of the prototype used for evaluating the thermal resistances, are reported in Table 1.

Table 2 reports the values of the thermal resistances along the main heat transfer paths. The resistances are evaluated starting from the geometrical data of the prototype and silicon oil data sheet. The comparison between the manufacturer data relative to air cooling and the obtained resistance results is reported is reported in Table 2.

In particular, the thermal network model of Fig. 3 can be simplified and the following thermal resistances can be defined:

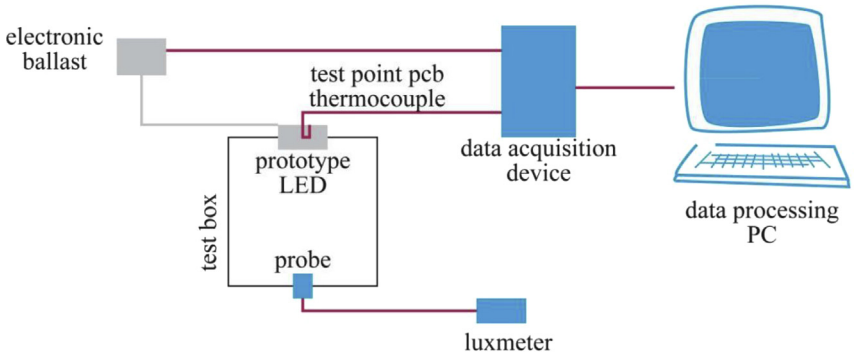

Fig. 5. Schematic presentation of experimental setup for the thermal and optical performance of the LED lighting system.

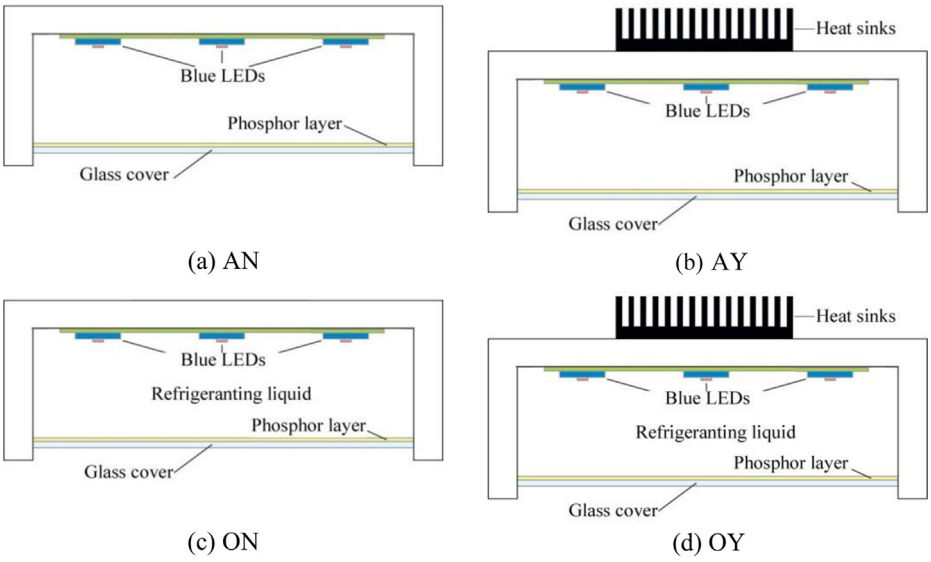

Fig. 7. The four experimentally investigated configurations.

- thermal resistance through the PCB, R_{PCB}:

$$R_{PCB} = \frac{R_1 \cdot R_2}{R_1 + R_2} \tag{11}$$

The value of R_{PCB} is 1.5 times lower than the junction to board thermal resistance reported by the manufacturer.

- R_{axial} is the thermal resistance from the fluid in the case and the surroundings through the phosphor glass, and can be expressed as:

$$R_{axial} = R_5 + R_6 + R_7 \tag{12}$$

- R_{radial} is the thermal resistance from the fluid in the case and the surroundings, through the sides of the case and the mounting flanges and can be expressed as:

$$R_{radial} = R_3 + R_4 + \frac{1}{\frac{1}{R_8} + \frac{1}{R_9} + \frac{1}{R_{10}}} \tag{13}$$

Finally, the junction to ambient thermal resistance can be expressed as:

$$R_{tot} = R_{PCB} + \frac{1}{\frac{1}{R_{axial}} + \frac{1}{R_{radial}}} \tag{14}$$

The percentage relative difference between the manufacturer data and the silicon fluid conditions can be expressed as:

$$D = \frac{R_{lc} - R_{ac}}{R_{ac}} \cdot 100 \tag{15}$$

Based on the results reported in Table 2, the junction to board thermal resistance is about 33% lower, while the junction to ambient thermal resistance is reduced by at least 19%.

4. Experimental method

The fabricated prototype performances are investigated in terms of illuminance output, voltage applied to the LEDs, electric current absorbed by the LEDs, and operating temperatures of the LED junctions. The experimental system setup established for the thermal and optical performance of the LED lighting system is shown in Fig. 5.

The illuminance was measured by a portable luxmeter (uncertainty ±1%) and two readings were recorded: one at the start of the

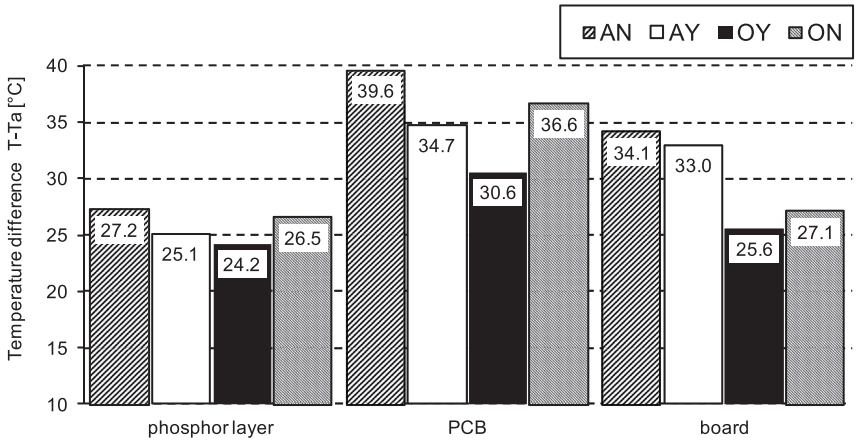

Fig. 8. Measured temperature differences of the 4 experimentally tested configurations.

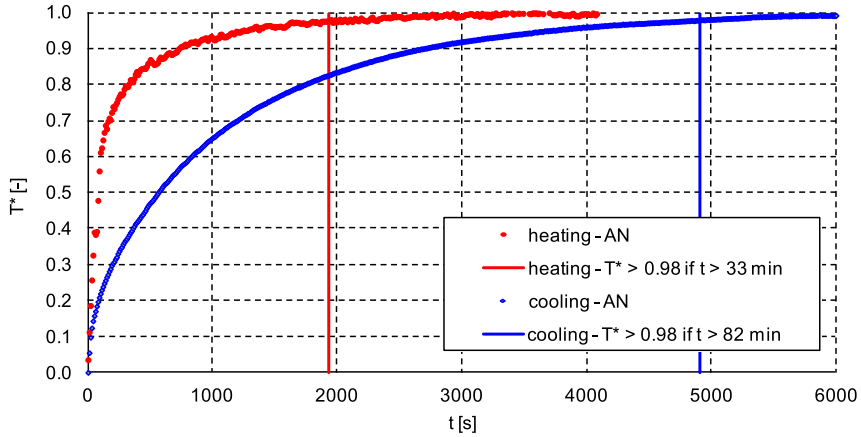

Fig. 9. Variation of T^* in time during the heating and cooling transient processes.

experiment (single reading), and the other in steady state conditions (three values averaged).

Other characteristics of the light radiation emitted by the prototype (color temperature and color rendering index) were not analyzed, as previous investigations have shown that the silicon liquid does not significantly influence the emission spectrum of the LED used [19]. In fact, as illustrated in Fig. 6, the 440–460 nm wavelength range in which the blue Rebel LED emits is not subject to cuts by the refrigerating silicon liquid. Thus, the color temperature and the color rendering index can be considered the same in all investigated configurations.

For the electrical and thermal measurements, a digital multimeter connected to a PC was used to record and store data, with a sampling frequency of 0.1 Hz during the entire duration of the conducted experiment (heating, steady state operation, and cooling).

The voltage measurement was carried out directly by the digital multimeter (uncertainty 1%), while the measurements of electrical current and temperatures were indirect. The electrical current is converted into voltage by a Hall effect transducer and measured by a digital multimeter (uncertainty 1%). The temperature was measured by thermocouples (uncertainty ±0.2 °C).

The conducted experiments had the purpose to investigate the influence of heat sink and refrigerating fluid (between the LEDs and the glass with phosphor) on the previous presented measures. A rectangular aluminum plate heat sink a (side length 40 mm, thickness 1.5 mm) and a matrix (12 rows × 12 columns) of pins (height 16 mm, width 1.75 mm, and thickness 1.2 mm) has been used. Two refrigerating fluids were used: air and silicon oil (Dow Corning PV-6010 [20]). As consequence, four experimental configurations were and denoted as shown in Fig. 7:

(a) AN: cooling fluid Air; heat sink installed: No;
(b) AY: cooling fluid: Air; heat sink installed: Yes;
(c) ON: cooling fluid: silicon Oil; heat sink installed: No;
(d) OY: cooling fluid: silicon Oil; heat sink installed: Yes.

4.1. Thermal test results and discussions

The temperature measurements were carried out, for all the different configurations of Fig. 7, in some different points for providing information on the temperature of different system's components. In particular:

a) on the LED test point to indirectly determine the junction temperature. According to the manufacturer, the LED junction temperature is evaluated as [22]:

$$T_j = T_b + P \cdot R_{\theta_{j-b}} \tag{16}$$

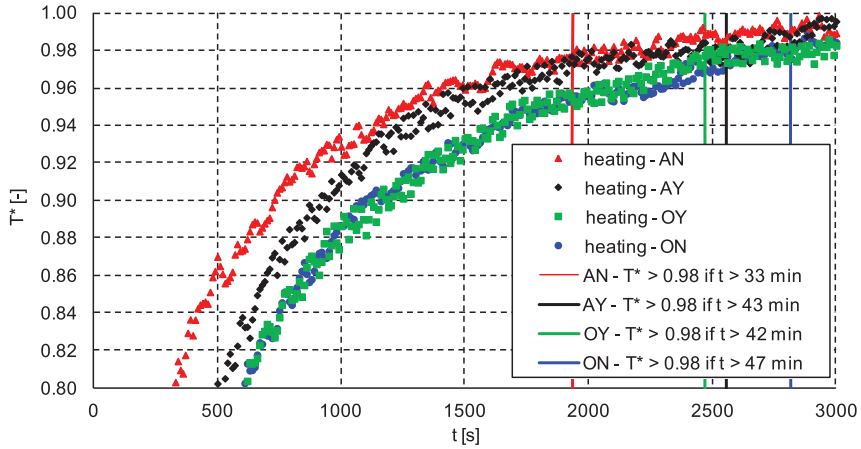

Fig. 10. Heating transient and transient time for the four experimented configurations.

Table 3
Time transient of heating and cooling process.

Experimented configuration	Heating transient [min]	Cooling transient [min]
AN	33	82
AY	43	78
OY	42	96
ON	47	110

Table 4
Measured illuminance of lamp prototype at switch on, and in steady state.

Configuration	Switch on [lux]	Steady state [lux]
AN	42.5	41.3
AY	42.5	41.4
OY	42.8	42.0
ON	43.8	41.8

where, T_b is the LED temperature on the board test point, T_j the junction temperature, P is the LED power, and $R_{\theta j-b}$ is the known thermal resistance junction-to-board;

b) on the inner part of the glass cover, where the phosphor layer is placed;
c) at the center of the PCB board;
d) outside the prototype in the surrounding ambient.

The system, initially switched off, is electrically supplied. All the temperatures and electrical measures were recorded. The ending points of the transient processes are established based on the measured temperatures, and can be expresses as:

- for the heating transient process:

$$0.99 \leq \frac{T_i - T_{air,i}}{\frac{\sum_i^{i+60} T_i}{60} - T_{air,i}} \leq 1.01 \tag{17}$$

- for the cooling transient process:

$$0.99 \leq \frac{(T_s - T_i)}{T_s - T_{air,i}} \leq 1.01 \tag{18}$$

where T_i is the generic lamp temperature at i-th sample, $T_{air,i}$ is the generic air temperature at i-th sample, and T_s is the generic lamp temperature in steady state. The values of reported temperatures are the averaged values of 60 samples (10 min acquisition interval).

Fig. 8 shows the obtained results in steady state condition. Configuration OY, with refrigerating silicon oil and heat sink, reports the lowest operating temperature. This occurs because the air acts like a thermal insulator, the combined effect of the heat sink that reduces the thermal resistance with the surrounding air, and the refrigerating silicon oil inside the lamp, which is more suitable than air as heat transfer fluid. Moreover, the heat sink has a larger effect on temperature reduction as oil, as the configuration AY has a lower operating temperature than configuration ON. The surrounding temperature T_{air} was about 19.6 °C during all the tests.

For comparing the obtained results during the heating and cooling transients, two dimensionless temperatures were used, expressed as:

$$T^* = \frac{T(t) - T_{air}(t + \Delta T)}{T(t + \Delta T) - T_{air}(t + \Delta T)} \quad \text{for heating} \tag{19}$$

$$T^* = \frac{T(t) - T(0)}{T_{air}(t + \Delta T) - T(0)} \quad \text{for cooling} \tag{20}$$

where $T(t + \Delta T)$ is the average temperature calculated based on the values recorded from time instant t to time instant $t + \Delta T$ ($\Delta T = 10$ min). The steady state condition is set-up when $T^* > 0.98$.

In the following analysis, the LED experimentally recorded temperatures on the LED test point T_b will be used for illustrating the variation of T^* in time, during the heating and cooling transient processes. For exemplification, the heating and cooling transients for the AN prototype (operating with Air and with No heat sink) are illustrated in Fig. 9, as the trend is similar for all the operating conditions.

Fig. 10 shows a comparison of the heating transient times for the four different LED configurations experimented.

Table 3 reports the time required to reach the steady state condition for the heating and cooling ($T^* > 0.98$) of the experimented configurations. The results reveal that the transient time is shorter in case of heating with respect to cooling. The difference could be determined by the higher heat transfer coefficient provided by the free convection on the board, which is immediately activated by the almost instantaneous warming of the LEDs. Furthermore, the transient times increase in the presence of oil due to the larger heat capacity of oil with respect to air. Finally, the experimentally tests of OY configuration reveals heating and cooling transients 30% longer than configuration AY (characterized by the shortest transient time).

Fig. 11. Black box for experimentally determination of illuminance.

The comparison between experimental results and simulated equivalent circuit model described in Section 3 is carried out. In particular, considering the junction-to-air temperature difference of the two configurations AN and ON, we have:

$$D = \frac{R_{j-a}(ON) - R_{j-a}(AN)}{R_{j-a}(AN)} \cdot 100 = -20.0\% \quad (21)$$

The result is in good agreement with the value of the heat transfer model reported in Table 3, and predicting a percentage reduction in the junction-to-air thermal resistance exceeding 19.5%.

The power consumption is about 12 W for all the four experimented configurations (AN, AY, OY, and ON).

4.2. Luminous radiation test results and discussions

The light radiation tests were performed considering only the quantity of light emitted from the prototype (illuminance in a specific point), investigating if lower operating temperatures guarantee higher luminous efficiency. The quality of light (emission spectrum, color temperature, and color rendering index) was not investigated as already analyzed in a previous work [19]. In particular, the illuminance of LED spotlight at point *P* was experimentally investigated (as shown Fig. 11).

The LED prototype was suspended at the center of the top face of a 1 cubic meter opaque black box. The probe of the luxmeter was placed at the center of the box's bottom face. The illuminance was recorded at the time instant of the prototype switch on, when the heating transient process was completed. Each measurement was repeated for three times, at time intervals of 10 s of each other.

Table 4 reports the illuminance obtained results, revealing that the behavior of the bright spot is consistent with what was expected. Although, with variations not particularly significant, the illuminance generated by the OY and ON prototypes are exceeding the air-based tested configurations.

5. Conclusions

A new fabricated lamp prototype, based on blue LEDs and using silicon fluid as cooling liquid, is theoretically analyzed and experimentally validated for assessing the thermal and luminous performances. Four different configurations (air/silicon oil as cooling agent, and with/without heat sink) were investigated. The experimental results reveal that the combination of heat sink and refrigerating liquid provides the most efficient thermal dissipation. Hence, longer lifetime of the components can be achieved. Still, the heating and cooling transients increase. A compromise between the heat dissipation and transient process duration should be addressed. Consequently, the heat sink successful design and careful sizing of refrigerating volume should be performed. The pc LEDs guarantees high luminous efficiency and uniform white light emission of the source. In addition, a small increase in light flux is achieved too.

References

[1] A. Dolara, S. Leva, Power quality and harmonic analysis of end user devices, Energies 5 (2012) 5453–5466.
[2] R. Faranda, S. Guzzetti, G.C. Lazaroiu, S. Leva, LEDs lighting: two case studies, UPB Sci. Bull. C 73 (2011) 199–210.
[3] B.J. Huang, C.W. Tang, Thermal–electrical–luminous model of multi-chip polychromatic LED luminaire, Appl. Therm. Eng. 29 (2009) 3366–3373.
[4] J. Li, B. Ma, R. Wang, L. Han, Study on a cooling system based on thermoelectric cooler for thermal management of high-power LEDs, Microelectron. Reliab. 51 (2011) 2210–2215.
[5] J.H. Choi, M.W. Shin, Thermal investigation of LED lighting module, Microelectron. Reliab. 52 (2012) 830–835.
[6] S.H. Yu, K.S. Lee, S.J. Yook, Natural convection around a radial heat sink, Int. J. Heat Mass Transf. 53 (2010) 2935–2938.
[7] T. Cheng, X.B. Luo, S.Y. Huang, Thermal analysis and optimization of multiple LED packaging based on a general analytical solution, Int. J. Therm. Sci. 49 (2010) 196–201.
[8] K.C. Yung, H. Liem, H.S. Choy, Z.X. Cai, Thermal investigation of a high brightness LED array package assembly for various placement algorithms, Appl. Therm. Eng. 63 (2014) 105–118. http://dx.doi.org/10.1016/j.applthermaleng.2013.11.009.
[9] P. Anithambigai, K. Dinashi, D. Mutharasu, S. Shanmugan, C.K. Lim, Thermal analysis of power LED employing dual interface method and water flow as a cooling system, Thermochim. Acta 523 (2011) 237–244.
[10] C.P. Ching, M. Devarajan, Study on thermal and optical properties of high power infrared emitter by utilizing dual interface method, Int. J. Heat Mass Transf. 58 (2013) 578–584.
[11] P. Schlotter, R. Schmidt, J. Schneider, Luminescence conversion of blue light emitting diodes, Appl. Phys. A 64 (1997) 417–418.
[12] J. Hwang, Y. Kim, J. Kim, S. Jung, H. Kwon, T. Oh, Study on the effect of the relative position of the phosphor layer in the LED package on the high power LED lifetime, Phys. Status Solidi C 7 (7–8) (2010) 2157–2161.
[13] B. Yan, N.T. Tran, J. You, F.G. Shi, Can junction temperature alone characterize thermal performance of white LED emitters? IEEE Phot. Technol. Lett. 23 (2011) 555–557.
[14] R. Hu, X.B. Luo, H. Zheng, Hotspot location shift in the high power phosphor converted white light-emitting diode package, Jpn. J. Appl. Phys. 51 (2012) 09MK05.
[15] X. Luo, X. Fu, F. Chen, H. Zheng, Phosphor self-heating in phosphor converted light emitting diode packaging, Int. J. Heat Mass Transf. 58 (2013) 276–281.
[16] B.-J. Huang, C.-W. Tang, M.-S. Wu, System dynamics model of high-power LED luminaire, Appl. Therm. Eng. 29 (2009) 609–616.
[17] J. Li, F. Lin, D. Wang, W. Tian, A loop-heat-pipe heat sink with parallel condensers for high-power integrated LED chips, Appl. Therm. Eng. 56 (2013) 18–26.
[18] B. Ramos-Alvarado, B. Feng, G.P. Peterson, Comparison and optimization of single-phase liquid cooling devices for the heat dissipation of high-power LED arrays, Appl. Therm. Eng. 59 (2013) 648–659.
[19] R. Faranda, S. Guzzetti, G.C. Lazaroiu, S. Leva, Refrigerating liquid prototype for LED's thermal management, Appl. Therm. Eng. 48 (2012) 155–163.
[20] Dow Corning 561 Silicon Transformer Liquid – Technical Manual, Dow Corning Corporation, 2006 (Available on line www.xiameter.com).
[21] F. Incropera, D.P. De Witt, T.L. Bergmann, A.S. Lavine, Fundamentals of Heat and Mass Transfer, sixth ed., John Wiley & Sons, New York, 2006.
[22] L. Jayasinghe, Y. Gu, N. Narendran, Characterization of thermal resistance coefficient of high-power LEDs, Proc. SPIE 6337 (2006) 1–10.